

# From Limited Labels to Open Domains: An Efficient Learning Method for Drone-view Geo-Localization

Zhongwei Chen, *Student Member, IEEE*, Zhao-Xu Yang, *Member, IEEE*, Hai-Jun Rong, *Senior Member, IEEE*, Jiawei Lang, Guoqi Li, *Member, IEEE*

**Abstract**—Traditional supervised drone-view geo-localization (DVGL) methods heavily depend on paired training data and encounter difficulties in learning cross-view correlations from unpaired data. Moreover, when deployed in a new domain, these methods require obtaining the new paired data and subsequent retraining for model adaptation, which significantly increases computational overhead. Existing unsupervised methods have enabled to generate pseudo-labels based on cross-view similarity to infer the pairing relationships. However, geographical similarity and spatial continuity often cause visually analogous features at different geographical locations. The feature confusion compromises the reliability of pseudo-label generation, where incorrect pseudo-labels often drive negative optimization. Given these challenges inherent in both supervised and unsupervised DVGL methods, we propose a novel cross-domain invariant knowledge transfer network (CDIKTNet) with limited supervision, whose architecture consists of a cross-domain invariance sub-network (CDIS) and a cross-domain transfer sub-network (CDTS). This architecture facilitates a closed-loop framework for invariance feature learning and knowledge transfer. The CDIS is designed to learn cross-view structural and spatial invariance from a small amount of paired data that serves as prior knowledge. It endows the shared feature space of unpaired data with implicit cross-view correlations at initialization, which alleviates feature confusion. Based on this, the CDTS employs dual-path contrastive learning in a shared feature space. Extensive experiments demonstrate that CDIKTNet achieves state-of-the-art performance under full supervision compared with those supervised methods, and further surpasses existing unsupervised methods in both few-shot initialization and cross-domain initialization setting.

**Index Terms**—drone-view geo-localization, structural invariance learning, spatial invariance learning, knowledge transfer.

## I. INTRODUCTION

CROSS-VIEW geo-localization has emerged as a promising visual localization technique [1]. Early efforts primarily focus on retrieving ground-view images to geo-referenced satellite imagery for ground-view geo-localization

This paper is submitted for review on November 27, 2025. This work was supported in part by the Key Research and Development Program of Shaanxi, PR China (No. 2023-YBGY-235), the National Natural Science Foundation of China (No. 61976172 and No. 12002254), Major Scientific and Technological Innovation Project of Xianyang, PR China (No. L2023-ZDKJ-JSGG-GY-018). (Corresponding author: Zhao-Xu Yang and Hai-Jun Rong)

Zhongwei Chen, Zhao-Xu Yang, Hai-Jun Rong and Jiawei Lang are with the State Key Laboratory for Strength and Vibration of Mechanical Structures, Shaanxi Key Laboratory of Environment and Control for Flight Vehicle, School of Aerospace Engineering, Xi'an Jiaotong University, Xi'an 710049, PR China (e-mail: ISChenawei@stu.xjtu.edu.cn; yangzhx@xjtu.edu.cn; hjrong@mail.xjtu.edu.cn). Guoqi Li is with the Institute of Automation, Chinese Academy of Sciences, Beijing 100190, China, also with the School of Artificial Intelligence, University of Chinese Academy of Sciences, Beijing 101408, China, and also with the Peng Cheng Laboratory, Shenzhen 518000, China (e-mail: guoqi.li@ia.ac.cn).

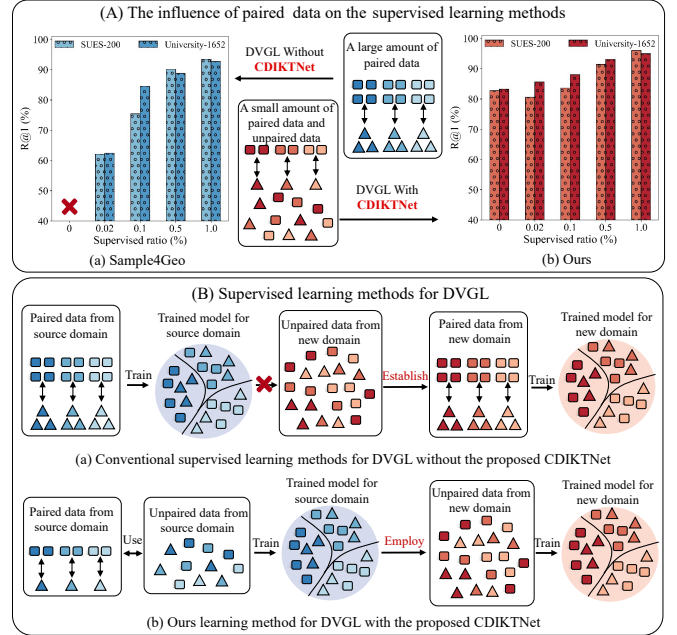


Fig. 1. **CDIKTNet VS. State-of-the-Art Supervised Methods.** (A) The performance variations of the representative method Sample4Geo[5] and CDIKTNet under different proportions of paired data are analyzed in the drone→satellite scenario using University-1652[9] and SUES-200[10] datasets. The evaluation on SUES-200 is performed at an altitude of 150m. It is evident that Sample4Geo generally underperforms CDIKTNet. Specifically, at a 0% supervision ratio, Sample4Geo becomes completely ineffective, whereas CDIKTNet continues to show its effectiveness. (B) Existing supervised methods are at risk of failure when transferred to a new domain if paired data is unavailable, as they heavily rely on such data for adaptation. In contrast, CDIKTNet can adapt to new domains without requiring explicit pairing.

[2]. With the widespread adoption of drones in complex scenarios such as emergency response [3] and urban surveys [4], the demand for autonomous localization in GPS-denied environments has been steadily increasing. This has driven more research interests in drone-view geo-localization (DVGL) [5, 6]. However, the dynamic viewpoints of drones result in scale distortions and non-rigid spatial transformations compared with satellite imagery. This pronounced structural and spatial heterogeneity presents challenges for DVGL. In recent years, benefiting from previous research efforts [7, 8], supervised DVGL methods with paired data have made notable progress. These paired data often require manual labeling, which provides an accurate pairing relationship between satellite imagery and drone images of the same location.

However, as illustrated in Fig. 1 (A(a)) and (B(a)), existing supervised methods [11–13] strictly rely on a large amount of

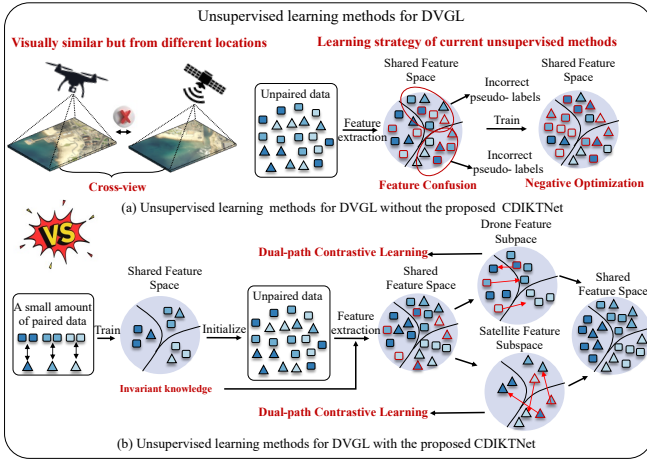


Fig. 2. **CDIKTNet vs. State-of-the-Art Unsupervised Methods.** (a) Spatial continuity causes visually similar patterns from different locations. Unsupervised methods often encounter feature confusion, which results in inaccurate pseudo-labels and drives negative optimization. (b) CDIKTNet leverages a small amount of paired data at initialization to learn cross-view invariance as prior knowledge. Based on this, it obtains a reliable shared feature space and further employs dual-path contrastive learning to optimize each subspace.

paired data to learn cross-view correlations. The absence of sufficient paired data leads to a dramatic decline in model performance. When the supervised ratio drops to 0, or in other words, when there is no paired data and all the data are unpaired, the existing supervised methods become ineffective. We mark this situation with a red X in the figures. Furthermore, dynamic drone mission environments often lead to domain shifts, which in turn require repeated efforts to re-establish cross-view correlations before deployment in new domains. It hinders the applicability in scenarios where pairing relationships are difficult to obtain and cross-domain adaptation is required. As shown in Fig. 1 (B(a)), the new domain where all data are unpaired cannot directly employ the trained model from the source domain. Therefore, researchers have increasingly focused on unsupervised methods for DVGL. Recent work [14] constructed a sparse 3D point cloud from multi-view drone images and rendered pseudo-satellite images with near-orthographic views via 3D Gaussian splatting to realize geometric transformations of the drone images. These synthetic images are then matched against real satellite imagery to enable unsupervised training. However, this method is sensitive to 3D reconstruction and pose estimation errors, and it is difficult to bridge the inherent cross-view domain gaps. In contrast, another work [15] utilizes a frozen pre-trained backbone and a learnable adapter to align features from different views in shared feature space. The shared feature space serves as a unified latent representation in which drone and satellite views can be directly aligned. Cross-view pseudo-labels are generated automatically based on feature similarity as supervised signals to guide training. This method avoids explicit geometric transformations and aims to intrinsically learn cross-view correlations. Nevertheless, as shown in Fig. 2 (a), when visually similar patterns appear at different geographical locations, the resulting feature confusion in the shared feature space often leads to incorrect pseudo-label generation. This

ultimately drives the model toward negative optimization.

In this paper, we propose an efficient learning method with limited supervision for DVGL that mitigates the adverse effects of inaccurate pseudo-labels caused by feature confusion, called the cross-domain invariant knowledge transfer network (CDIKTNet). Specifically, the CDIKTNet consists of two core components, including the cross-domain invariance sub-network (CDIS) and the cross-domain transfer sub-network (CDTS). The CDIS utilizes a small amount of paired data to learn latent cross-view structural and spatial invariance, which serves as prior knowledge. As illustrated in Fig. 2(b), it endows the shared feature space of unpaired data with similar implicit cross-view correlations at initialization to alleviate feature confusion. Based on this, CDTS introduces dual-path contrastive learning to independently optimize subspaces under different views. Despite being optimized separately, these subspaces maintain alignment in the shared feature space due to the shared invariance prior. The main contributions can be summarized as follows.

- We propose a cross-domain invariant knowledge transfer network, which can leverage few-shot guided cross-view invariance learning to further explore latent cross-view correlations within unpaired data. It reduces reliance on strictly paired data and enables direct transfer to new domains without requiring any prior pairing information.
- The CDIS is designed to learn the structural and spatial invariance by integrating channel-wise local and global structural information, and performing joint interaction learning along the different dimensions of the features. It is utilized to construct a shared feature space with better consistency and compactness for subsequent unsupervised learning.
- The CDTS is built on the shared cross-view invariance prior, which enables unpaired data to form initial cross-view correlations in the shared feature space. On this basis, dual-path contrastive learning is employed to perform clustering and assign pseudo-labels within subspaces, which are then used as supervised signals to optimize the representations of each view.
- Three experimental settings are designed to encompass a spectrum of learning paradigms that span fully supervised learning and limited-supervision learning. In the context of limited supervised learning, the proportion of paired data and unpaired data is allowed for random variation. Specifically, the cross-domain initialization setting provides an effective learning paradigm for new domains without requiring any prior pairing information. Extensive experiments demonstrate that CDIKTNet outperforms existing supervised methods under full supervision and surpasses existing unsupervised methods in both few-shot initialization and cross-domain initialization setting.

Notably, as illustrated in Fig. 1(A(b)) and (B(b)), compared with supervised methods, CDIKTNet remains effective at varying levels of supervision and can be transferred to new domains without requiring paired data. Furthermore, as shown in Fig. 2, compared with unsupervised methods, CDIKTNet performs initial feature space optimization using limited paired

data. Meanwhile, it adopts dual-path contrastive learning to optimize each subspace, which reduces feature confusion.

The remainder of this paper is organized as follows. Section II systematically reviews previous research. In Section III, the proposed method is presented in detail. The experimental results are reported and analyzed in Section IV. Finally, conclusions are outlined in Section V.

## II. RELATED WORK

### A. Supervised Cross-view Geo-localization

Cross-view geo-localization (CVGL) is widely recognized as an image retrieval problem based on heterogeneous visual data. However, challenges arise from geometric-semantic heterogeneity and feature distribution shifts across different viewpoints. In traditional CVGL sub-tasks, such as ground-view geo-localization [16–18], many researchers have employed explicit geometric alignment methods [19–21] to enforce structural consistency at varying viewpoints, while others [22, 23] have used GANs [24] to map source domain images to the target domain. Moreover, in drone-view geo-localization, which is another core sub-task in CVGL, PCL [25] attempted to align aerial and satellite images using perspective projection transformation. It also employed GAN to synthesize satellite-style images in order to reduce spatial discrepancies. But it was difficult to handle non-rigid deformations caused by dynamic UAV viewpoints and remained constrained by the synthetic-to-real domain gap. Recently, researchers [26, 27] have begun to model latent geometric structures or spatial consistency to enhance the robustness of DVGL. Nevertheless, these methods often focused solely on optimizing geometric structures or spatial representations while neglecting their synergistic relationships. This results in limited generalization under scale variations and spatial shifts in the DVGL. Furthermore, these methods still rely on large amounts of paired data for training, which restricts their applicability in open environments.

Inspired by the aforementioned supervised learning methods, our method utilizes a small amount of paired data for initialization, and further exploits structural and spatial consistency under limited supervision to learn robust and generalizable cross-view representations. Compared with these supervised methods, our method significantly reduces the reliance on paired data while achieving superior performance.

### B. Unsupervised Cross-Domain Retrieval

In recent years, cross-domain image retrieval based on the supervised methods has made significant progress [28, 29]. CSCL [30] enhances cross-domain pedestrian matching by jointly leveraging structural alignment and semantic alignment to extract modality-invariant semantic cues. CSDN [31] mitigates the modality discrepancies by integrating visual features with high-level semantic information captured by CLIP [32] to enrich the cross-domain representation space. To address the severe performance degradation caused by occlusion, OAFR [33] simulates diverse occlusion patterns to enable the model to perceive OTP and PTP occlusions, and further reconstructs the occluded query features using the unoccluded gallery features, which leads to more robust cross-domain

retrieval performance. However, the reliance on large-scale annotated data has limited its applicability. Fortunately, recent advances in domain adaptation [34–36] and semi/unsupervised learning [37–39] have demonstrated that robust representations can be learned even under weak or missing labels. This research trend provides important insights for extending cross-domain retrieval toward unsupervised settings and has motivated researchers to explore unsupervised cross-domain retrieval methods [40–42]. Current methods [43–45] utilized powerful feature backbone networks for feature initialization, employing clustering algorithms [46] to generate pseudo-labels and feature queues that provide stable negative samples for optimizing feature learning. However, these methods are primarily designed for homogeneous data with strong correlations, and their effectiveness tends to degrade significantly when applied to heterogeneous scenarios. To address the limitations, some researchers [47, 48] have proposed cross-modal person retrieval methods based on dual-path contrastive learning. Nevertheless, these methods still depend on pre-trained person retrieval models for feature extraction during initialization.

To better learn cross-view correlations, we adopt a pseudo-label-based training scheme using unpaired data, where pseudo-labels are generated through clustering in accordance with the methods described above. In contrast, the model is initialized with a small amount of paired data. It leads to a more compact and discriminative feature space and enables more reliable pseudo-label generation. Notably, although unsupervised DVGL can also be considered an unsupervised cross-domain retrieval task, existing methods remain limited and have already been discussed in the Introduction. We refrain from repeating the details here.

## III. PROPOSED METHOD

**Problem Formulation.** Given a drone-view image set  $\mathcal{X}^d = \{x_i^d\}_{i=1}^N$  and a satellite-view image set  $\mathcal{X}^s = \{x_j^s\}_{j=1}^M$ , where each drone image  $x_i^d$  is paired with a corresponding satellite image  $x_j^s$  as a positive pair  $(x_i^d, x_j^s)$ , the objective is to learn a shared feature space  $\mathcal{V}$  that minimizes the distance between positive pairs while maximizing the distance between negative pairs. Existing methods heavily rely on a large amount of paired data as positive samples for training to achieve high performance. In contrast, our method fundamentally differs by mitigating this dependency. The following sections provide a detailed explanation of our method.

### A. Cross-Domain Invariance Sub-network

The CDIS lies in the complementarity between structural and spatial invariance. In DVGL, variations in viewpoint and scale are significant. Therefore, it is necessary to learn the structural and spatial features that are invariant to varying viewpoints and scales. This structural invariance consists of local geometric information, like corners, edges, and contours, and global structural information, such as spatial layout and domain-invariant topologies. Additionally, spatial invariance is derived from the scale-aware contextual cues.

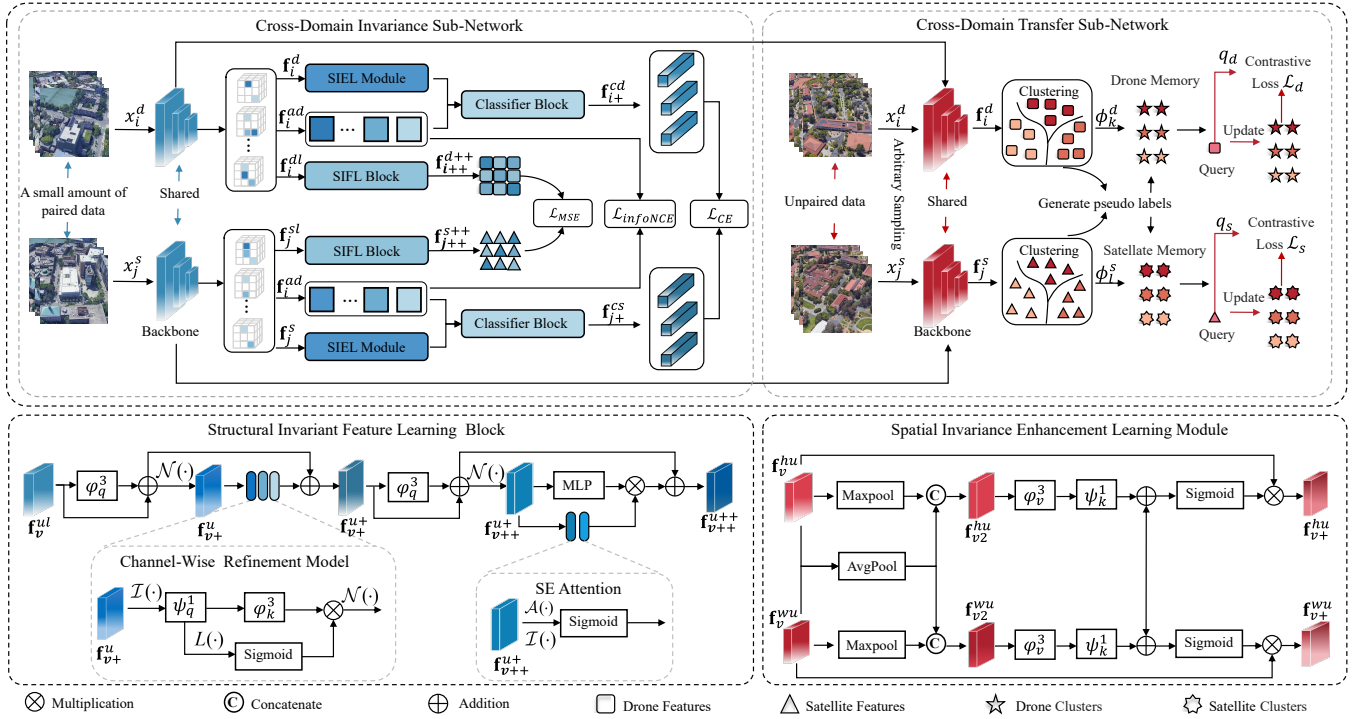


Fig. 3. **Pipeline Overview.** The proposed network pipeline consists of two sub-networks. The cross-domain invariance sub-network is designed to learn feature representations that exhibit structural invariance and spatial invariance. The cross-domain transfer sub-network utilizes the invariant knowledge learned by the cross-domain invariance sub-network as a feature representation space to further explore the latent correlations of cross-view from unpaired data.

1) *Structural Invariant Learning (SIFL) Block:* Given a pair of cross-view images  $\{x_i^d, x_j^s\}$ , high-dimensional feature representations are first extracted using the ConvNeXt-Base [49] backbone network. The extracted features are represented as  $\mathbf{f}_v^u \in \mathbb{R}^{C \times H \times W}$ , where  $u \in \{d, s\}$ . Specifically,  $v$  is defined as follows: when  $u = d$ ,  $v = i$  and when  $u = s$ ,  $v = j$ . To effectively leverage structural features at different viewpoints, the dimensions  $H \times W$  are flattened into a single dimension  $L$  to obtain the features  $\mathbf{f}_v^{ul} \in \mathbb{R}^{C \times L}$ .  $\mathbf{f}_v^{ul}$  serves as the input to the SIFL block.

Subsequently, a depthwise separable  $3 \times 3$  convolution  $\varphi_q^3$  is used to mine local structural priors, while residual connections preserve the original topological information. After normalization  $\mathcal{N}(\cdot)$ , the feature representation  $\mathbf{f}_{v+}^u$  can be obtained. To further enhance the capability of structural invariance feature learning, we proposed a channel-wise refinement (CWR) module. Specifically, we project  $\mathbf{f}_{v+}^u$  into the latent space through two cascaded linear transformation layers  $\mathcal{I}(\cdot)$  to learn high-order interactions between channels. A subsequent  $1 \times 1$  convolution  $\psi_q^1$  is applied to explicitly learn local structural features.

Following this, a gating mechanism  $\mathcal{G}(\cdot)$  consists of a depthwise separable  $3 \times 3$  convolution  $\varphi_k^3$  branch and a linear transformation branch  $L(\cdot)$ , which is performed the channel-wise selective enhancement via a sigmoid activation. Then, the residual connection and normalization  $\mathcal{N}(\cdot)$  are employed to fuse cross-layer information to enhance representation. This process can be formulated as

$$\mathbf{f}_{v+}^u = \mathcal{N}(\varphi_q^3(\mathbf{f}_v^{ul}) + \mathbf{f}_v^{ul}) \quad (1)$$

$$\mathbf{f}_{v+}^{u+} = \mathcal{N}(\mathcal{G}(\psi_q^1(\mathcal{I}(\mathbf{f}_{v+}^u)))) + \varphi_q^3(\mathbf{f}_v^{ul}) + \mathbf{f}_v^{ul}. \quad (2)$$

To further enhance local geometric information, we adopt the same feature processing procedure as in Eq. 1 to extract the feature  $\mathbf{f}_{v++}^{u+}$ . Although  $\mathbf{f}_{v++}^{u+}$  contains rich local geometric information, it still lacks global structural features. Therefore, we replace the CWR module described previously with an MLP  $\mathcal{P}(\cdot)$  combined with the squeeze-and-excitation (SE) attention [50]. In this process, the global average pooling  $\mathcal{A}(\cdot)$  is first applied within the SE attention to extract the global information at the channel level. The channel information is then compressed through two linear transformation layers  $\mathcal{I}^+(\cdot)$ , followed by the channel attention weights calculated using the sigmoid function  $\mathcal{F}$ , which are then combined with the global channel information obtained through the MLP. This further enhances the expression of global channel-level information. Finally, a residual connection is used to fuse the rich local channel-level information from the original features with the enhanced global information. This process can be formulated as

$$\mathbf{f}_{v++}^{u+} = \mathcal{N}(\varphi_q^3(\mathbf{f}_{v+}^{u+}) + \mathbf{f}_{v+}^{u+}) \quad (3)$$

$$\mathbf{f}_{v+++}^{u++} = \mathcal{F}(\mathcal{I}^+(\mathcal{A}(\mathbf{f}_{v++}^{u+}))) \times \mathcal{P}(\mathbf{f}_{v++}^{u+}) + \varphi_q^3(\mathbf{f}_{v+}^{u+}) + \mathbf{f}_{v+}^{u+}. \quad (4)$$

2) *Spatial Invariant Enhancement Learning (SIEL) Module:* Spatial information is particularly crucial for DVGL. To enhance spatial invariance, inspired by [11], we design a dual-path spatial invariance enhancement learning module to mine spatial information from different dimensions.

In the spatial invariance enhancement learning module, we preserve the dimensions, namely height  $H$  and weight  $W$  of the input features. By permuting the input features

$\mathbf{f}_v^u \in \mathbb{R}^{C \times H \times W}$  along the channel-height (C-H) and channel-width (C-W) dimensions, we obtain  $\mathbf{f}_v^{hu} \in \mathbb{R}^{H \times C \times W}$  and  $\mathbf{f}_v^{wu} \in \mathbb{R}^{W \times H \times C}$ , respectively. This allows the module to capture multi-perspective dependencies from different dimensions. Subsequently, global feature representations  $\mathbf{f}_{v2}^{hu} \in \mathbb{R}^{2 \times C \times H}$  and  $\mathbf{f}_{v2}^{wu} \in \mathbb{R}^{2 \times W \times C}$  are generated by concatenating the results of max pooling and average pooling applied to the permuted features. A  $3 \times 3$  depthwise separable convolution  $\varphi_v^3$  and a separate  $1 \times 1$  convolution  $\psi_k^1$  are then employed to obtain a more compact feature representation. Subsequently, cross-interaction across the C-H and C-W is performed to further enhance the spatial invariance of the feature representation. Finally, the fused features are normalized using a sigmoid function  $\mathcal{F}$  to generate attention weights, which are multiplied with the original feature maps and restored to the original dimensions  $\mathbb{R}^{C \times H \times W}$ , yielding the spatially enhanced feature  $\mathbf{f}_{v+}^{hu} \in \mathbb{R}^{C \times H \times W}$  and  $\mathbf{f}_{v+}^{wu} \in \mathbb{R}^{C \times H \times W}$  as

$$\mathbf{f}_{v+}^{hu} = \mathcal{F}(\psi_k^1(\varphi_v^3(\mathbf{f}_{v2}^{hu})) + \psi_k^1(\varphi_v^3(\mathbf{f}_{v2}^{wu}))) \times \mathbf{f}_v^{hu} \quad (5)$$

$$\mathbf{f}_{v+}^{wu} = \mathcal{F}(\psi_k^1(\varphi_v^3(\mathbf{f}_{v2}^{wu})) + \psi_k^1(\varphi_v^3(\mathbf{f}_{v2}^{hu}))) \times \mathbf{f}_v^{wu}. \quad (6)$$

3) *Multi-level Optimization*: In the CDIS, the features  $\mathbf{f}_{v++}^{u++}$  obtained from the SIFL are optimized using the mean squared error loss  $\mathcal{L}_{MSE}$  [13], which improves the stability and consistency of the learned features. Furthermore, to enhance structural representation in the spatial invariance enhancement learning module, the features  $\mathbf{f}_v^{au}$  are first extracted by the backbone and processed via global average pooling. The features  $\mathbf{f}_v^{au}$  combined with  $\mathbf{f}_{v+}^{hu}$  and  $\mathbf{f}_{v+}^{wu}$ , and the resulting combination are passed through a classifier module [11] to obtain  $\mathbf{f}_{v+}^{cu}$ . Subsequently,  $\mathbf{f}_{v+}^{cu}$  are optimized with cross-entropy loss  $\mathcal{L}_{CE}$  to enhance feature discrimination and cross-view consistency. In addition, to further enhance the feature representations,  $\mathbf{f}_v^{au}$  undergo independent optimization using InfoNCE loss [51]  $\mathcal{L}_{InfoNCE}$ . The final objective is to minimize the sum of all losses. It can be formulated as

$$\mathcal{L}_1 = \lambda_1 \mathcal{L}_{MSE} + \lambda_2 \mathcal{L}_{CE} + \lambda_3 \mathcal{L}_{InfoNCE} \quad (7)$$

where  $\lambda_1$ ,  $\lambda_2$  and  $\lambda_3$  are the coefficients to control the relative importance of the loss terms.

*Remark 1*: The CDIS lies in dual optimization of structural and spatial invariance. On one hand, it integrates local and global structural information along the channel dimension and is guided by  $\mathcal{L}_{MSE}$  to effectively constrain the feature search space, which enhances the structural representations. On the other hand, CDIS retains the original spatial dimensions and performs joint interaction learning along C-H and C-W, where  $\mathcal{L}_{CE}$  is employed to further mine scale-aware contextual cues. This structure-spatial collaborative modeling enables the CDIS to achieve rapid convergence and learn highly discriminative representations, even with limited paired data.

### B. Cross-Domain Transfer Sub-network

The CDTS further explores cross-view correlations based on the enhanced consistency and compactness established by the CDIS. Specifically, the CDTS incorporates dual-path contrastive learning tailored explicitly for DVGL.

1) *Cross-View Feature Memory Initialization*: As shown in Fig. 3, at the beginning of each training epoch, we initialize cross-view feature instances using the invariant knowledge learned by the CDIS and perform clustering to generate pseudo-labels. This process aims to mitigate the issue of low-quality pseudo-label initialization caused by suboptimal feature extraction. Subsequently, we construct cluster memories for each view, specifically for drone and satellite perspectives denoted as  $\phi_k^d$  and  $\phi_l^s$ , by computing the average feature representations of drone and satellite instances within each cluster. This process can be formulated as

$$\phi_k^d = \frac{1}{|\mathcal{H}_k^d|} \sum_{\mathbf{f}_i^d \in \mathcal{H}_k^d} \mathbf{f}_i^d, \phi_l^s = \frac{1}{|\mathcal{H}_l^s|} \sum_{\mathbf{f}_j^s \in \mathcal{H}_l^s} \mathbf{f}_j^s \quad (8)$$

where  $\mathbf{f}_i^d$  and  $\mathbf{f}_j^s$  are drone and satellite instance features, respectively.  $i = 1, \dots, N$ ,  $j = 1, \dots, M$ .  $\mathcal{H}_k^d$  and  $\mathcal{H}_l^s$  denote the  $k$ -th cluster set in drone and  $l$ -th cluster satellite view, respectively.  $|\cdot|$  indicates the number of instances per cluster.

*Remark 2*: In selecting the clustering algorithm, we refer to several unsupervised cross-domain retrieval works [45, 52] and adopt DBSCAN [46] for clustering. Unlike partition-based methods such as K-means [53], DBSCAN utilizes a density-based method, which handles clusters of arbitrary shapes and noisy data. It does not require a predefined number of clusters, nor does it force all points to be assigned to a cluster. Additionally, DBSCAN can identify and exclude noise points, which ensures the selection of valid samples even in cross-view challenges

2) *Cross-View Feature Memory Updating*: During each training iteration, the cluster memories using a momentum updating strategy are represented as

$$\phi_k^{d(\omega)} \leftarrow \alpha \phi_k^{d(\omega-1)} + (1 - \alpha) q_d \quad (9)$$

$$\phi_l^{s(\omega)} \leftarrow \alpha \phi_l^{s(\omega-1)} + (1 - \alpha) q_s \quad (10)$$

where  $\alpha$  is momentum updating factor and  $\omega$  is iteration number.  $q_d$  and  $q_s$  represent the given query features of the drone and the satellite, respectively.

3) *Cross-View Contrastive Loss*: Given the drone and satellite query  $q_d$  and  $q_s$ , we compute the contrastive loss for the drone view and the satellite view as

$$\mathcal{L}^d = -\log \frac{\exp(q_d \cdot \phi_+^d / \tau)}{\sum_{k=0}^K \exp(q_d \cdot \phi_k^d / \tau)} \quad (11)$$

$$\mathcal{L}^s = -\log \frac{\exp(q_s \cdot \phi_+^s / \tau)}{\sum_{l=0}^L \exp(q_s \cdot \phi_l^s / \tau)} \quad (12)$$

where  $\tau$  denotes the temperature hyper-parameter. Drone cluster memories  $\phi_k^d$  and satellite cluster memories  $\phi_l^s$  are utilized as feature vectors at the cluster level to compute the distances between the query instance  $q_{d(s)}$  and all clusters. Here,  $\phi_+^d$  and  $\phi_+^s$  correspond to the positive cluster memory associated with  $q_d$  and  $q_s$ , respectively.

*Remark 3*: Benefiting from CDIS, instances  $\mathbf{f}_i^d$  and  $\mathbf{f}_j^s$  exhibit stronger compactness within their respective subspaces and cross-view correlation in shared feature space. This also makes  $\phi_k^d$  and  $\phi_l^s$  more representative and an initial alignment in the shared feature space. On this basis,  $\mathcal{L}^d$  and  $\mathcal{L}^s$  further guide each instance feature towards its corresponding  $\phi_k^d$  and

TABLE I  
COMPARISONS BETWEEN EXISTING STATE-OF-THE-ART METHODS AND  
CDIKTNET ON UNIVERSITY-1652.

		University-1652					
Setting	Model	GT Ratio (%)	Drone→Satellite		Satellite→Drone		
			R@1	AP	R@1	AP	
i	MuSe-Net[6]	100	74.48	77.83	88.02	75.10	
	TransFG[54]	100	84.01	86.31	90.16	84.61	
	IFSs[26]	100	86.06	88.08	91.44	85.73	
	MCCG[11]	100	89.40	91.07	95.01	89.93	
	Sample4Geo[5]	100	92.65	93.81	95.14	91.39	
	CAMP[7]	100	94.46	95.38	96.15	92.72	
	DAC[13]	100	94.67	95.50	<b>96.43</b>	93.79	
	CDIKTNet	100	<b>95.02</b>	<b>95.79</b>	<b>96.15</b>	<b>93.93</b>	
ii	CDIKTNet	10	88.02	89.84	93.87	86.48	
	CDIKTNet	2	85.63	87.75	90.44	82.24	
UM	EM-CVGL[15]	0	70.29	74.93	79.03	61.03	
iii	CDIKTNet	0	<b>83.30</b>	<b>85.73</b>	<b>87.73</b>	<b>76.53</b>	

<sup>1</sup>“UM” is employed as the abbreviated form of “Unsupervised Method”.

$\phi_l^s$  within the subspace, thereby indirectly facilitating cross-view alignment in the shared feature space.

The CDTS is jointly optimized with  $\mathcal{L}^d$  and  $\mathcal{L}^s$ . Thus, the final optimization for CDIKTNet is denoted as  $\mathcal{L} = \mathcal{L}_1 + \mathcal{L}^d + \mathcal{L}^s$ .

#### IV. EXPERIMENTAL RESULTS

##### A. Datasets and Evaluation Protocol

We evaluate CDIKTNet on two challenging benchmarks for DVGL. University-1652 dataset [9] consists of drone, satellite, and ground-view images from 1,652 locations in 72 universities. Its training set includes 701 buildings from 33 universities, while the test set comprises 951 buildings from 39 universities. SUES-200 dataset [10] comprises 200 locations, which are split into 120 for training and 80 for testing. Each location provides a satellite image and drone images taken at four different altitudes, which encompass diverse environments such as parks, lakes, and buildings. We employ Recall@K (R@K) and Average Precision (AP) as evaluation metrics. Additionally, Ground Truth Ratio (GT ratio) denotes the proportion of paired data within the entire experimental dataset.

##### B. Implementation Details

During training and testing, all input images are resized to  $3 \times 384 \times 384$ . The CDIS is trained for 1 epoch, while the CDTS runs for 30 epochs, with a batch size of 64. In DBSCAN, the neighborhood radius is set to 0.40 and 0.30 for drone-view images and satellite-view images, respectively, and the minimum number required to form a cluster is 4. AdamW optimizer is used for the CDIS with an initial learning rate of 0.001, followed by SGD optimization for the CDTS with a learning rate of 0.00025. Furthermore, in Eq.(7),  $\lambda_1$ ,  $\lambda_2$ , and  $\lambda_3$  are set to 0.6, 0.1, and 1, respectively. The CDTS is activated only when there exists unpaired data.

##### C. Comparison with State-of-the-art Methods

We conduct experiments with three settings, namely (i) fully supervised learning, (ii) few-shot initialization, and (iii) cross-domain initialization. The methods under comparison

encompass a range of state-of-the-art techniques. For supervised learning, these include MuSe-Net [6], TransFG [54], IFSs [26], MCCG [11], Sample4Geo [5], CAMP [7] and DAC [13]. In the realm of unsupervised learning, the methods are EM-CVGL [15], SegVLAD [56], AnyLoc [55] and Li [14]. Notably, SegVLAD [56], AnyLoc [55] and Li [14] are reported in separate Tables IV, V and VI due to the absence of complete results in their publications.

**(i) Fully Supervised Learning:** In this setting, we utilize all paired data, where the proportion of such paired data accounts for 100% as shown in Tables I and II. Compared with existing state-of-the-art methods, CDIKTNet in this setting achieves superior performance on both dataset. Specifically, on University-1652, it attains 95.02% R@1 and 95.79% AP in the evaluation scenario of drone→satellite. Although it ranks second in the evaluation scenario of satellite→drone, it still attains the highest AP. On SUES-200, in two evaluation scenarios and at four altitudes, CDIKTNet generally outperforms the advanced supervised methods such as DAC [13] and CAMP [7] and significantly surpasses Sample4Geo [5]. Furthermore, as shown in Table III, CDIKTNet trained in this setting demonstrates superior generalization capability compared with state-of-the-art supervised methods when these methods trained on University-1652 are tested on SUES-200. These results validate the effectiveness of CDIKTNet.

**(ii) Few-shot Initialization:** To evaluate the effectiveness of CDIKTNet in leveraging unlabeled data for learning, we initialize CDIKTNet with only 2% and 10% of the paired data. The remaining training data are entirely unpaired. As shown in Tables I and II, CDIKTNet with only 2% of the paired data achieves performance comparable to or even surpassing that of IFSs [54]. With 10% of paired data, CDIKTNet achieves further improvements, surpassing most fully supervised methods and achieving performance comparable to MCCG [11]. Notably, as shown in Table III, CDIKTNet in this setting trained with only 10% of the paired data exhibits even stronger generalization than these fully supervised methods.

Furthermore, compared with state-of-the-art unsupervised methods, including EM-CVGL [15], AnyLoc [55], SegVLAD [56], and Li [14], as illustrated in Tables I, II, IV and V, CDIKTNet in this setting significantly outperforms them in all metrics on both datasets, despite relying on only a small proportion of paired data. In terms of generalization, CDIKTNet still significantly surpasses these methods, as reported in Tables III and VI. This underscores the significance of employing a limited quantity (e.g., 2%) of paired data for initialization, as it serves to steer the exploration toward revealing deeper cross-view representations from unpaired data.

**(iii) Cross-domain Initialization:** We propose a novel experimental setting for cross-domain validation. We initialize CDIKTNet with 2% of paired data and then conduct the training process with the remaining unpaired data on one dataset that corresponds to a specific domain. This trained model is then transferred to another dataset representing a distinct domain for further training without requiring additional pairing relationships, with 0% of paired data during the transfer phase. Therefore, in this setting, the GT ratio is marked as 0%.

The reverse validation follows the same procedure. As

TABLE II  
COMPARISONS BETWEEN EXISTING STATE-OF-THE-ART METHODS AND CDIKTNET ON SUES-200.

		SUES-200																
Setting	Model	GT Ratio (%)	Drone → Satellite								Satellite → Drone							
			150m				200m				250m				300m			
			R@1	AP	R@1	AP	R@1	AP	R@1	AP	R@1	AP	R@1	AP	R@1	AP		
i	IFSs [26]	100	77.57	81.30	89.50	91.40	92.58	94.21	97.40	97.92	93.75	79.49	97.50	90.52	97.50	96.03	<b>100.00</b>	97.66
	MCCG[11]	100	82.22	85.47	89.38	91.41	93.82	95.04	95.07	96.20	93.75	89.72	93.75	92.21	96.25	96.14	98.75	96.64
	Sample4Geo[5]	100	92.60	94.00	97.38	97.81	98.28	98.64	99.18	99.36	97.50	93.63	98.75	96.70	98.75	98.28	98.75	98.05
	DAC[13]	100	<b>96.80</b>	<b>97.54</b>	97.48	97.97	98.20	98.62	97.58	98.14	97.50	94.06	98.75	96.66	98.75	98.09	98.75	97.87
	CAMP[7]	100	95.40	96.38	97.63	98.16	98.05	98.45	99.33	99.46	96.25	93.69	97.50	<b>96.76</b>	98.75	98.10	<b>100.00</b>	<b>98.85</b>
ii	CDIKTNet	10	83.60	86.24	90.53	92.14	94.33	95.32	97.13	97.60	91.25	83.24	95.00	89.53	97.50	93.59	97.50	95.80
	CDIKTNet	2	80.55	83.58	88.05	90.10	91.28	93.13	94.48	96.12	90.00	77.16	91.25	85.92	97.50	91.36	97.50	94.07
UM	EM-CVGL[15]	0	55.23	60.80	60.95	61.03	68.10	72.62	74.42	78.20	73.75	54.00	91.25	65.65	96.25	72.02	97.50	74.74
iii	CDIKTNet	0	<b>82.75</b>	<b>85.25</b>	<b>89.35</b>	<b>91.13</b>	<b>93.15</b>	<b>94.39</b>	<b>95.18</b>	<b>96.12</b>	<b>88.75</b>	<b>80.33</b>	<b>93.75</b>	<b>88.17</b>	<b>95.00</b>	<b>92.15</b>	<b>98.75</b>	<b>94.37</b>

TABLE III  
COMPARISONS BETWEEN EXISTING STATE-OF-THE-ART METHODS AND CDIKTNET TRAINED IN SETTING I AND II IN GENERALIZATION CAPACITY.

		University-1652 → SUES-200																
Setting	Model	GT Ratio (%)	Drone → Satellite								Satellite → Drone							
			150m				200m				250m				300m			
			R@1	AP	R@1	AP	R@1	AP	R@1	AP	R@1	AP	R@1	AP	R@1	AP		
i	MCCG[11]	100	57.62	62.80	66.83	71.60	74.25	78.35	82.55	85.27	61.25	53.51	82.50	67.06	81.25	74.99	87.50	80.20
	Sample4Geo[5]	100	70.05	74.93	80.68	83.90	87.35	89.72	90.03	91.91	83.75	73.83	91.25	83.42	93.75	89.07	93.75	90.66
	DAC[13]	100	76.65	80.56	86.45	89.00	92.95	94.18	94.53	95.45	87.50	79.87	<b>96.25</b>	88.98	95.00	92.81	<b>96.25</b>	<b>94.00</b>
	CAMP[7]	100	78.90	<b>82.38</b>	86.83	89.28	91.95	93.63	<b>95.68</b>	<b>96.65</b>	87.50	78.98	95.00	87.05	95.00	91.05	<b>96.25</b>	93.44
	CDIKTNet	100	<b>80.20</b>	<b>81.20</b>	<b>88.85</b>	<b>90.65</b>	<b>93.32</b>	<b>94.51</b>	<b>94.10</b>	<b>95.16</b>	<b>90.00</b>	<b>82.85</b>	<b>93.75</b>	<b>89.92</b>	<b>96.25</b>	<b>92.48</b>	<b>95.00</b>	<b>93.62</b>
ii	CDIKTNet	10	81.35	84.28	89.15	91.16	94.18	95.29	96.68	97.32	91.25	81.10	97.50	90.44	98.75	93.87	98.75	95.05
	CDIKTNet	2	70.98	75.15	80.18	83.47	87.05	89.36	87.05	94.37	81.25	71.05	92.50	81.20	92.50	87.60	96.25	91.49
UM	EM-CVGL[15]	0	60.03	65.69	71.50	76.17	80.35	83.85	85.93	88.34	73.75	56.99	87.50	70.62	92.50	81.18	95.00	86.04
iii	CDIKTNet	0	<b>79.08</b>	<b>82.55</b>	<b>90.07</b>	<b>91.85</b>	<b>93.05</b>	<b>94.37</b>	<b>95.00</b>	<b>95.95</b>	<b>86.25</b>	<b>77.90</b>	<b>92.50</b>	<b>86.40</b>	<b>93.75</b>	<b>90.16</b>	<b>95.00</b>	<b>92.22</b>

TABLE IV  
COMPARISONS BETWEEN EXISTING STATE-OF-THE-ART UNSUPERVISED METHODS AND CDIKTNET ON UNIVERSITY-1652.

		University-1652					
Setting	Model	GT Ratio (%)	Drone → Satellite				
			R@1	R@5	R@10	AP	
UM	AnyLoc[55]	0	42.08	57.92	69.19	-	
	SegVLAD[56]	0	68.19	77.32	77.18	-	
	Li(a)[14]	0	57.49	73.32	77.18	-	
	Li(b)[14]	0	76.60	80.46	84.88	-	
ii	CDIKTNet	10	88.02	89.84	93.87	86.48	
	CDIKTNet	2	85.63	94.86	96.31	87.75	
iii	CDIKTNet	0	<b>83.30</b>	<b>94.00</b>	<b>95.71</b>	<b>85.73</b>	

<sup>2</sup>Li(a)[14] and Li(b)[14] correspond to different parameter configurations reported in the original paper.

TABLE V  
COMPARISONS BETWEEN EXISTING STATE-OF-THE-ART UNSUPERVISED METHODS AND CDIKTNET ON SUES-200

		SUES-200					
Setting	Model	GT Ratio (%)	Drone → Satellite				
			200m		300m		
			R@1	AP	R@1	AP	
UM	AnyLoc[55]	0	34.00	46.74	41.00	51.94	
	SegVLAD[56]	0	69.50	72.98	73.00	74.26	
	Li(a)[14]	0	56.00	60.50	62.00	65.00	
	Li(b)[14]	0	73.00	76.54	76.50	77.52	
ii	CDIKTNet	10	89.15	91.16	96.68	97.32	
	CDIKTNet	2	88.05	90.10	94.48	96.12	
iii	CDIKTNet	0	<b>89.35</b>	<b>91.13</b>	<b>95.18</b>	<b>96.12</b>	

shown in Tables I, II, IV and V, after training in one domain, CDIKTNet can be directly transferred to another domain. It outperforms state-of-the-art unsupervised methods in all metrics and achieves performance comparable to several fully supervised methods. Moreover, as reported in Tables

TABLE VI  
COMPARISONS BETWEEN EXISTING STATE-OF-THE-ART UNSUPERVISED METHODS AND CDIKTNET TRAINED IN SETTING II IN GENERALIZATION CAPACITY.

		University-1652 → SUES-200									
Setting	Model	GT Ratio (%)	Drone → Satellite								
			150m		200m		250m		300m		
			R@1	AP	R@1	AP	R@1	AP	R@1	AP	
UM	AnyLoc[55]	0	30.00	42.74	34.00	46.74	36.78	50.41	41.00	51.97	
	SegVLAD[56]	0	56.00	59.08	69.50	72.98	72.50	74.10	73.00	74.26	
	Li(b)[14]	0	66.00	69.98	73.00	76.54	73.50	75.15	76.50	77.52	
ii	CDIKTNet	10	81.35	84.28	89.15	91.16	94.18	95.29	96.68	97.32	
	CDIKTNet	2	70.98	75.15	80.18	83.47	87.05	89.36	87.05	94.37	
iii	CDIKTNet	0	<b>79.08</b>	<b>82.55</b>	<b>90.07</b>	<b>91.85</b>	<b>93.05</b>	<b>94.37</b>	<b>95.00</b>	<b>95.95</b>	

III and VI, CDIKTNet demonstrates remarkable generalization performance. It significantly outperforms these state-of-the-art unsupervised methods. Notably, as shown in V, the experimental results in this setting demonstrates superior performance compared with the few-shot initialization setting, which utilizes 2% of paired data. This indicates that strong domain adaptability enables the cross-domain initialization setting to outperform limited paired supervision under some cases.

*Remark 4:* The (ii) few-shot initialization setting and (iii) cross-domain initialization setting are two typical scenarios of limited supervision. The former targets the current domain by utilizing a limited amount of paired data for initialization, which is a process of supervised learning. Subsequently, unpaired data is employed for unsupervised learning. The latter addresses the issue of a complete lack of paired data in a new domain. It first performs initialization through supervised learning in an existing domain using a limited amount of

TABLE VII  
COMPARISONS BETWEEN EXISTING STATE-OF-THE-ART METHODS AND CDIKTNET ON SUES-200 WITH 2% AND 10% PAIRED DATA.

SUES-200																		
Setting	Model	GT Ratio (%)	Drone → Satellite								Satellite → Drone							
			150m		200m		250m		300m		150m		200m		300m		300m	
			R@1	AP	R@1	AP	R@1	AP	R@1	AP	R@1	AP	R@1	AP	R@1	AP	R@1	AP
-	Sample4Geo[5]	2	62.10	68.11	69.85	74.93	74.85	79.14	76.40	80.33	77.50	57.91	88.75	70.17	91.25	76.99	90.00	78.89
	CAMP[7]	2	54.73	61.70	62.30	68.39	65.83	71.42	68.40	73.58	68.75	49.25	82.50	60.49	87.50	68.79	91.25	74.43
	DAC[13]	2	55.83	62.16	68.50	73.25	73.38	77.34	74.70	78.64	70.00	51.09	85.00	61.59	90.00	70.53	91.25	74.63
ii	CDIKTNet	2	<b>80.55</b>	<b>83.58</b>	<b>88.05</b>	<b>90.10</b>	<b>91.28</b>	<b>93.13</b>	<b>94.48</b>	<b>96.12</b>	<b>90.00</b>	<b>77.16</b>	<b>91.25</b>	<b>85.92</b>	<b>97.50</b>	<b>91.36</b>	<b>97.50</b>	<b>94.07</b>
-	Sample4Geo[5]	10	75.43	79.21	84.20	86.70	87.18	89.40	89.63	91.61	91.25	76.89	92.50	82.76	96.25	86.60	96.25	89.23
	CAMP[7]	10	76.27	80.39	83.83	86.89	89.66	91.62	90.85	92.71	92.50	77.50	96.25	86.63	97.50	91.45	97.50	93.29
	DAC[13]	10	76.80	80.65	85.05	87.65	88.80	90.81	90.58	92.32	<b>93.75</b>	<b>79.06</b>	<b>97.50</b>	<b>86.78</b>	<b>97.50</b>	<b>90.58</b>	<b>98.75</b>	<b>92.54</b>
ii	CDIKTNet	10	<b>83.60</b>	<b>86.24</b>	<b>90.53</b>	<b>92.14</b>	<b>94.33</b>	<b>95.32</b>	<b>97.13</b>	<b>97.60</b>	<b>91.25</b>	<b>83.24</b>	<b>95.00</b>	<b>89.52</b>	<b>97.50</b>	<b>93.59</b>	<b>97.50</b>	<b>95.80</b>

<sup>3</sup>“-” denotes the scenario where supervised methods are applied under limited paired relationships.

TABLE VIII  
COMPARISONS BETWEEN EXISTING STATE-OF-THE-ART METHODS AND CDIKTNET ON UNIVERSITY-1652 WITH 2% AND 10% OF PAIRED DATA.

University-1652						
Setting	Model	GT Ratio (%)	Drone → Satellite		Satellite → Drone	
			R@1	AP	R@1	AP
-	Sample4Geo[5]	2	62.41	66.85	84.45	60.52
	CAMP[7]	2	62.53	67.01	83.31	59.26
	DAC[13]	2	63.68	68.16	87.59	61.26
ii	CDIKTNet	2	<b>85.63</b>	<b>87.75</b>	<b>90.44</b>	<b>82.24</b>
-	CAMP[7]	10	83.64	86.27	92.44	82.27
	Sample4Geo[5]	10	84.51	86.94	93.01	83.53
	DAC[13]	10	84.64	87.07	93.15	83.03
ii	CDIKTNet	10	<b>88.02</b>	<b>89.84</b>	<b>93.87</b>	<b>86.48</b>

TABLE IX  
INFLUENCE OF EACH COMPONENT ON PERFORMANCE OF CDIKTNET.

University-1652							
	SIFL	SIEL	CDTS	Drone → Satellite		Satellite → Drone	
				R@1	AP	R@1	AP
2%				58.19	62.69	82.45	56.95
	✓			59.00	63.55	81.16	55.03
		✓		59.73	64.16	80.03	57.35
	✓	✓		63.93	68.19	83.45	61.35
	✓	✓	✓	<b>85.63</b>	<b>87.75</b>	<b>90.44</b>	<b>82.24</b>
100%				92.80	94.00	95.01	91.83
	✓			94.02	94.96	95.72	93.16
		✓		93.26	94.36	95.58	92.15
	✓	✓		<b>95.02</b>	<b>95.79</b>	<b>96.15</b>	<b>93.93</b>

paired data. Then, it uses the remaining unpaired data for unsupervised learning. The obtained model is directly applied to unsupervised learning in the new domain, and has achieved remarkable results in the DVGL task in the new domain.

Furthermore, as shown in Tables VII and VIII, existing supervised methods strictly rely on paired data as positive samples and cannot use unpaired data. In contrast, CDIKTNet can effectively exploit a large amount of unpaired cross-view information to achieve better performance under such limited conditions. Additionally, CDIKTNet also achieves competitive performance with 100% of paired data equivalent to fully supervised learning. This highlights its excellent adaptability and generalization in different supervision levels.

#### D. Ablation Studies

**Effectiveness of CDIS.** As shown in Table IX, both the SIFL block and SIEL module contribute significantly to performance improvements with both 2% and 100% of paired data. When used individually, each component increases R@1 and AP, which demonstrates their individual effectiveness. Notably, their joint optimization yields further improvement, which validates the design of the CDIS. Specifically, SIFL enhances geometric invariance at different viewpoints by modeling structural priors, while SIEL improves spatial consistency by incorporating scale-aware contextual cues. These two components complement each other to enable CDIKTNet to construct a unified and robust cross-view shared feature space.

**Effectiveness of CDTs.** With 2% of paired data, the introduction of CDTs leads to an increase in R@1 from 63.93% to 85.63% and AP from 68.19% to 87.75% in the drone→satellite scenario, while also improving satellite→drone R@1 from

83.45% to 90.44% and AP from 61.35% to 82.24%. These gains clearly show the effectiveness of CDTs. Using the invariant knowledge learned by CDIS, CDTs enables a more effective mining of cross-view correlations from unpaired data. It makes CDIKTNet retain strong performance in conditions with scarce paired annotations.

#### E. Further Analysis

**Hyper-parameters Analysis of the loss coefficients.** We further investigate the influence of the loss coefficients  $\lambda_1$ ,  $\lambda_2$ , and  $\lambda_3$  in Eq. (7) on the University-1652 dataset. As shown in Fig. 4, all three hyper-parameters exhibit stable trends within reasonable ranges. For  $\lambda_1$ , our method achieves consistently strong performance for  $\lambda_3 \in [0.4, 0.8]$ , and overly small or large values weaken the contribution of this term. For  $\lambda_2$ , the best results are obtained around  $\lambda_2 = 0.10$ , while both smaller and larger values lead to slight performance degradation. For  $\lambda_1$ , the performance gradually improves as the weight increases from 0.40 to 1.00, and the best results are obtained when  $\lambda_3 = 1.00$ . Based on these observations, the best overall performance is achieved at  $\lambda_1 = 0.60$ ,  $\lambda_2 = 0.10$ , and  $\lambda_3 = 1.00$ , and therefore we adopt these coefficients in all subsequent experiments.

**Hyper-parameters Analysis of the  $\alpha$ .** To evaluate the influence of the  $\alpha$ , we give quantitative comparisons and report the results in Fig. 5. As shown in Fig. 5, increasing the momentum factor  $\alpha$  leads to degraded performance in drone→satellite and satellite→drone seniors. A larger  $\alpha$  slows the update of the cluster memories and reduces its ability

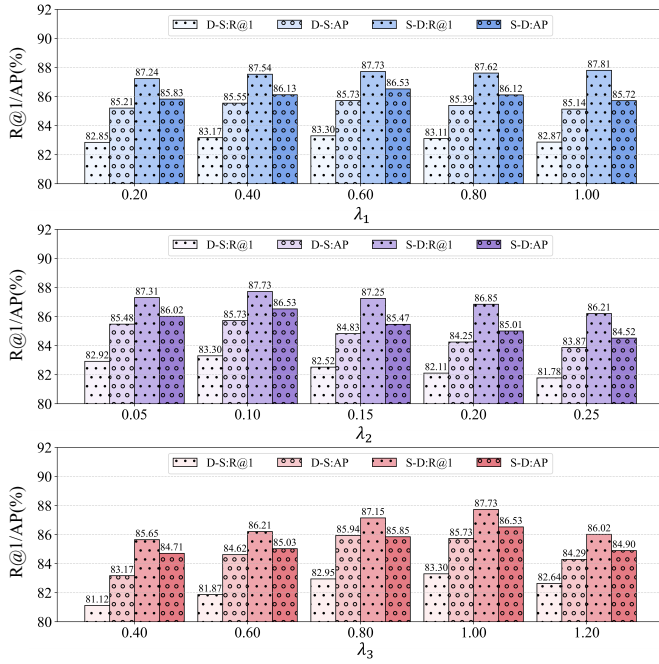


Fig. 4. **Performance Influence of  $\lambda_1, \lambda_2$  and  $\lambda_3$ .** Influence of different  $\lambda_1, \lambda_2$  and  $\lambda_3$  values on University-1652 in setting iii.

to adapt to cross-view variations. In contrast, CDTS requires rapid acquisition of cross-view cues, and a smaller  $\alpha$  assigns greater weight to new features, which allows CDTS to achieve faster adaptation.

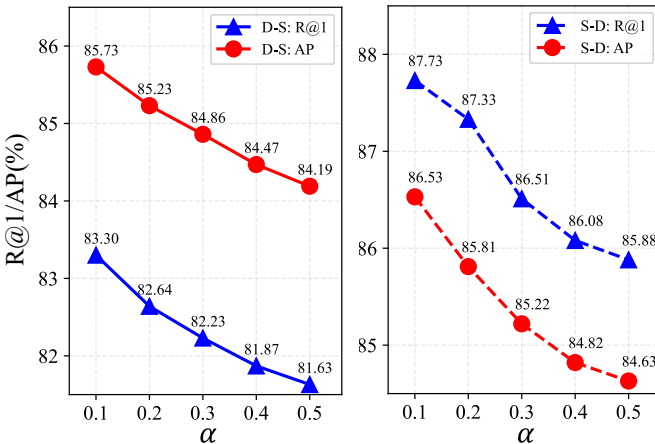
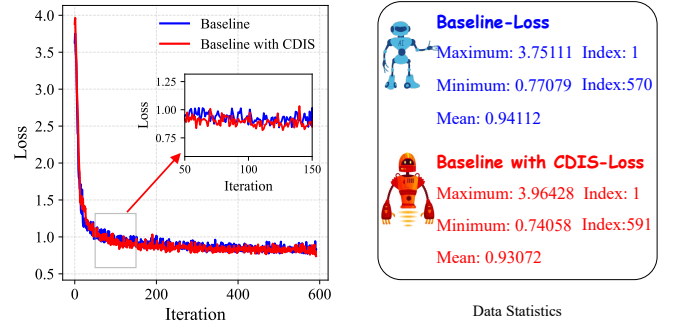
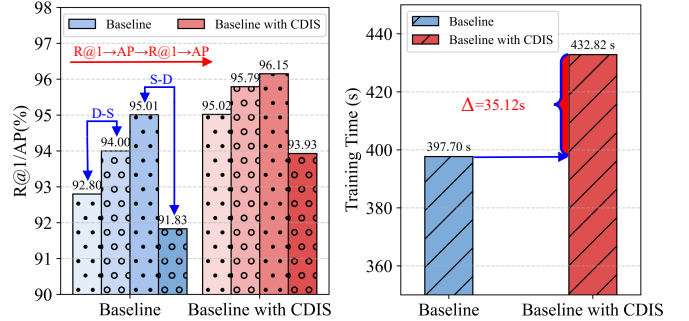


Fig. 5. **Performance Influence of  $\alpha$ .** Influence of different  $\alpha$  values on University-1652 in setting iii.

**Influence of CDIS on Convergence.** To further examine the influence of CDIS on convergence, we compare the training behavior of the baseline and baseline with CDIS on the University-1652 dataset in setting i. As shown in Fig. 6(a), it presents the loss curves and their statistical values. The baseline and baseline with CDIS follow similar descent patterns and show stable convergence regions. The baseline with CDIS begins with a slightly higher loss but reaches a lower final value, which demonstrates that the optimization process remains stable and that CDIS guides the model toward



(a) Loss Curves and Data Statistics



(b) Performance and Training Time

Fig. 6. **Influence of CDIS on Convergence, Performance, and Training Efficiency.** (a) Loss curves and statistical summaries for baseline vs. baseline with CDIS on University-1652 in setting i. (b) Comparison of performance and training time between baseline and baseline with CDIS on University-1652 in setting i.

a better solution. Fig. 6(b) reports the performance and the training time. CDIS improves the performance in both the drone  $\rightarrow$  satellite and satellite  $\rightarrow$  drone scenarios, and the additional training cost is small at about 35 seconds. These observations show that CDIS strengthens structural and spatial invariance without causing slower convergence and adds only a minor computational cost while achieves better performance.

**Method Effectiveness and Limitations Discussion.** To further validate the effectiveness of CDIKTNet, we introduced a more challenging dataset, DenseUAV [57], which focuses on low-altitude drone self-positioning. This dataset includes over 27,000 drone  $\rightarrow$  satellite images collected from 14 university campuses. DenseUAV presents significant challenges such as cross-view misalignment and spatial-temporal variations, with multi-scale satellite imagery and diverse temporal conditions.

As shown in Table X, in setting i, CDIKTNet surpasses most supervised methods despite the complexity of the dataset. In setting ii, Although sacrifices a small portion of paired data but greatly exceeds the performance of EM-CVGL. Moreover, in setting iii, CDIKTNet is initialized through cross-domain transfer using the University-1652 dataset. It still outperforms EM-CVGL. However, in settings ii and iii, CDIKTNet performs suboptimally compared to current supervised methods. The core challenge lies in the inherent confusion within the DenseUAV dataset, particularly the issues of cross-view misalignment and spatio-temporal variations. These challenges become more pronounced when paired data is limited during the initialization phase. Additionally, cross-domain initial-

ization requires the model to possess a certain degree of generalization ability from the source domain to the target domain for optimal initialization. This limitation highlights the importance of establishing strong prior knowledge during the initialization phase, which will significantly enhance cross-view alignment capabilities. In future work, we will explore methods that do not rely on such priors.

TABLE X  
COMPARISONS BETWEEN EXISTING STATE-OF-THE-ART METHODS AND CDIKTNET ON DENSEUAV

Setting	Model	GT Ratio (%)	DenseUAV							
			All height		80m		90m		100m	
			R@1	R@5	R@1	R@5	R@1	R@5	R@1	R@5
i	ConvNext-Tiny[57]	100	60.23	81.94	-	-	-	-	-	-
	Sample4Geo[5]	100	80.57	96.53	80.57	96.53	<b>86.87</b>	98.71	<b>91.38</b>	<b>99.74</b>
	DAC[13]	100	84.47	96.53	80.92	97.04	85.32	98.71	85.46	99.10
	CDIKTNet	100	<b>85.50</b>	<b>97.53</b>	<b>83.14</b>	<b>97.55</b>	<b>86.36</b>	<b>99.23</b>	<b>87.39</b>	<b>99.49</b>
ii	CDIKTNet	10	51.57	79.37	49.93	83.91	52.90	84.93	52.12	45.97
	CDIKTNet	2	39.76	72.11	39.00	75.55	39.64	78.77	39.90	80.31
UM	EM-CVGL	0	18.15	50.97	18.02	50.36	17.76	50.19	17.50	49.98
iii	CDIKTNet	0	<b>22.57</b>	<b>40.24</b>	<b>17.25</b>	<b>40.15</b>	<b>23.04</b>	<b>48.39</b>	<b>25.48</b>	<b>52.38</b>

### F. Visualization

As shown in Fig. 7, to further demonstrate the effectiveness of CDIKTNet, we visualize the similarity distribution using t-SNE [58] and feature space projection.

**Similarity Distribution Visualization.** As shown in Fig. 7(a–b), Sample4Geo and DAC achieve overlap areas of 0.1232 and 0.1124 under limited supervision, due to their inability to exploit unpaired data. Fig. 7(c) shows EM-CVGL [15] achieves an overlap of 0.1158. Although it performs slightly better, feature confusion remains an issue. In contrast, CDIKTNet in Fig. 7(d) achieves a lower overlap of 0.0661 with only 2% of paired data. This confirms its strong ability to align and separate cross-view features under limited supervision. Notably, in Fig. 7(e), CDIKTNet is trained in the cross-domain initialization setting described in Subsection IV-C. It still achieves an overlap of 0.0808 to outperform all methods. This shows its effectiveness in exploiting unpaired data and transferring knowledge from an external source domain.

**Feature Space Visualization.** In the feature space, features from the same location should cluster, while different locations should be well separated. As shown in Fig. 7(f–h), the compared methods show noticeable cross-view confusion (red circles) and dispersed feature distributions. In contrast, CDIKTNet (Fig. 7(i–j)) produces more compact and structured feature distributions in both scenarios. Although the 0% of paired data in cross-domain initialization setting shows minor confusion, the features remain more compact and more evenly aligned. This presents the ability of CDIKTNet in learning cross-view information.

**Attention Heatmap Visualization.** As a further demonstration of the effectiveness of SIEL, we visualize its attention heat maps in Fig. 8. Despite the large spatial differences between satellite and drone images and the feature distribution shifts caused by varying drone viewpoints, SIEL consistently highlights semantically meaningful regions in both views.

**Retrieval Visualization.** To visualize the effectiveness of CDIKTNet in cross-domain initialization setting, Fig. 9 shows retrieval results in both drone→satellite and satellite→drone

scenarios. CDIKTNet retrieves more correct matches than EM-CVGL [15], which demonstrates superior cross-view alignment and robustness to viewpoint variations.

## V. CONCLUSION

This paper addresses a critical and highly challenging problem in the drone-view geo-localization (DVGL) task with minimal or even no paired data to reduce dependence on expensive cross-view annotations. To this end, we propose a novel cross-domain invariant knowledge transfer network (CDIKTNet), which learns the spatial and structural invariance of cross-view features while constructing a robust invariant knowledge representation space. Meanwhile, it utilizes this shared space as an optimization anchor for unsupervised training, which effectively learns latent cross-view information from unpaired data. It significantly alleviates the reliance on paired data. More importantly, CDIKTNet can be applied under any level of supervision and can be generalized to new environments without requiring their prior pairing relationships. Extensive experiments demonstrate that, under full supervision, CDIKTNet outperforms existing state-of-the-art methods. Furthermore, when initialized with a small amount of paired data in the current domain or transferred to the other domain in the proposed cross-domain initialization setting, CDIKTNet outperforms state-of-the-art unsupervised methods and even surpasses some fully supervised methods. This advancement pushes DVGL closer to real-world deployment.

## REFERENCES

- [1] T. Shore, S. Hadfield, and O. Mendez, “BEV-CV: Birds-eye-view transform for cross-view geo-localisation,” in *Proc. IEEE/RSJ Int. Conf. Intell. Robots Syst.*, 2024, pp. 11 048–11 055.
- [2] S. Cai, Y. Guo, S. Khan, J. Hu, and G. Wen, “Ground-to-aerial image geo-localization with a hard exemplar reweighting triplet loss,” in *Proc. IEEE Int. Conf. Comput. Vis.*, 2019, pp. 8391–8400.
- [3] S. Liu, X. Li, H. Lu, and Y. He, “Multi-object tracking meets moving uav,” in *Proc. IEEE Conf. Comput. Vis. Pattern Recognit.*, 2022, pp. 8876–8885.
- [4] B. Li, Z. Huang, J. Ye, Y. Li, S. Scherer, H. Zhao, and C. Fu, “Pvt++: A simple end-to-end latency-aware visual tracking framework,” in *Proc. IEEE Int. Conf. Comput. Vis.*, 2023, pp. 10 006–10 016.
- [5] F. Deuser, K. Habel, and N. Oswald, “Sample4Geo: Hard negative sampling for cross-view geo-localisation,” in *Proc. IEEE Conf. Comput. Vis. Pattern Recognit.*, 2023, pp. 16 847–16 856.
- [6] T. Wang, Z. Zheng, Y. Sun, C. Yan, Y. Yang, and T.-S. Chua, “Multiple-environment self-adaptive network for aerial-view geo-localization,” *Pattern Recognit.*, vol. 152, p. 110363, 2024.
- [7] Q. Wu, Y. Wan, Z. Zheng, Y. Zhang, G. Wang, and Z. Zhao, “CAMP: Cross-view geo-localization method using contrastive attributes mining and position-aware partitioning,” *IEEE Trans. Geosci. Remote Sens.*, vol. 62, pp. 1–14, 2024.
- [8] Z. Chen, Z.-X. Yang, and H.-J. Rong, “Multilevel embedding and alignment network with consistency and invariance learning for cross-view geo-localization,” *IEEE Trans. Geosci. Remote Sens.*, vol. 63, pp. 1–15, 2025.
- [9] Z. Zheng, Y. Wei, and Y. Yang, “University-1652: A multi-view multi-source benchmark for drone-based geo-localization,” in *Proc. ACM Int. Conf. Multimedia*, 2020, p. 1395–1403.
- [10] R. Zhu, L. Yin, M. Yang, F. Wu, Y. Yang, and W. Hu, “SUES-200: A multi-height multi-scene cross-view image benchmark across drone and satellite,” *IEEE Trans. Circuits Syst. Video Technol.*, vol. 33, no. 9, pp. 4825–4839, 2023.
- [11] T. Shen, Y. Wei, L. Kang, S. Wan, and Y.-H. Yang, “MCCG: A convnext-based multiple-classifier method for cross-view geo-localization,” *IEEE Trans. Circuits Syst. Video Technol.*, vol. 34, no. 3, pp. 1456–1468, 2023.
- [12] H. Du, J. He, and Y. Zhao, “CCR: A counterfactual causal reasoning-based method for cross-view geo-localization,” *IEEE Trans. Circuits Syst. Video Technol.*, vol. 34, no. 11, pp. 11 630–11 643, 2024.

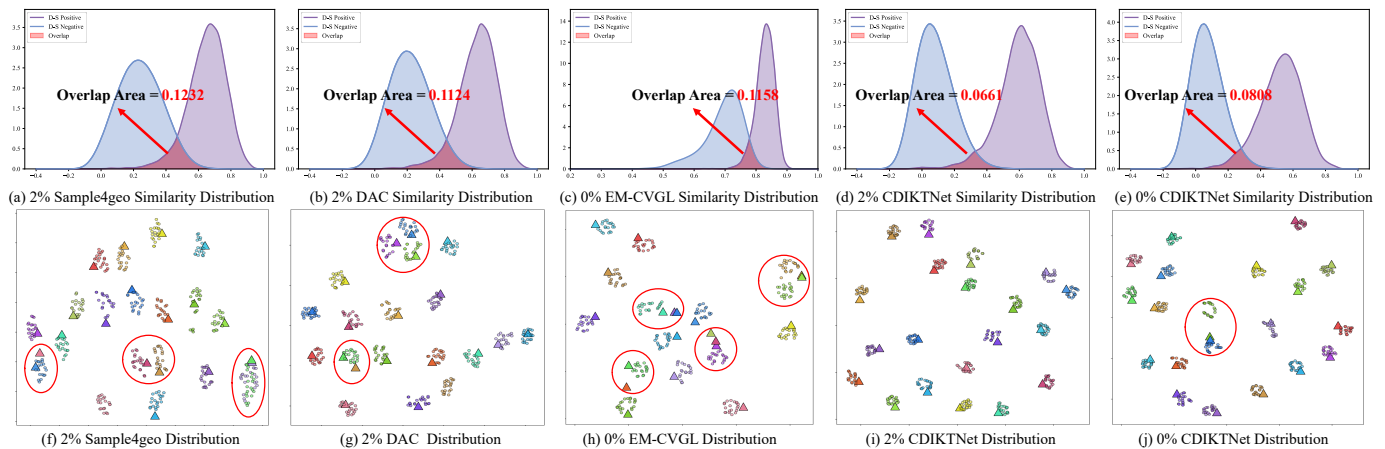


Fig. 7. **Similarity Distribution and Feature Space Visualization on University-1652**. (a–e) show the similarity distribution visualization. The red-shaded area indicates the overlapping region between the positive and negative distributions. (f–j) show the distribution of feature embeddings in the 2D shared feature space, where circles and triangles in different colors denote drone and satellite view. A total of 20 localizations are randomly selected from the test set.

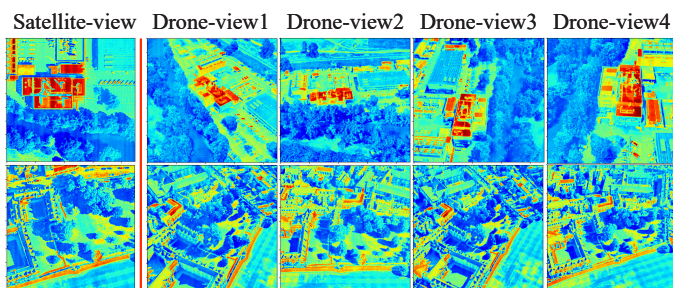


Fig. 8. **Attention Heatmap Visualization**. The attention responses generated by the proposed SIEL module are visualized. Red regions correspond to stronger attention responses, whereas blue regions denote weaker responses.

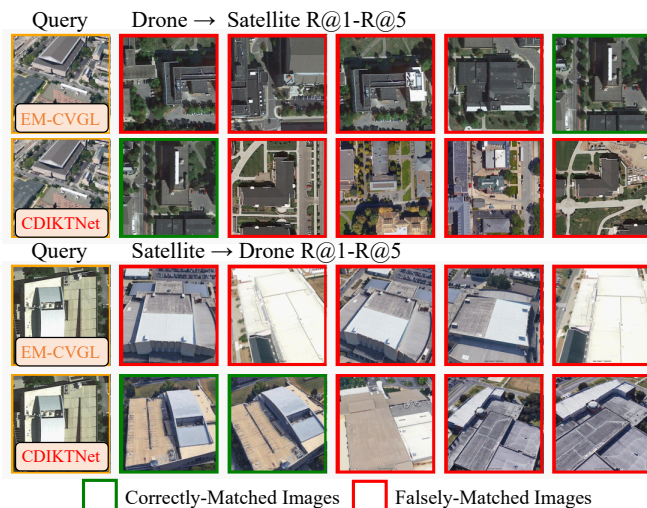


Fig. 9. **Retrieval Visualization on University-1652**. The green box indicates a correctly-matched image, and the red box indicates a falsely-matched image.

[13] P. Xia, Y. Wan, Z. Zheng, Y. Zhang, and J. Deng, “Enhancing cross-view geo-localization with domain alignment and scene consistency,” *IEEE Trans. Circuits Syst. Video Technol.*, pp. 1–12, 2024.

[14] H. Li, C. Xu, W. Yang, L. Mi, H. Yu, H. Zhang, and G.-S. Xia, “Unsupervised multiview uav image geolocation via iterative rendering,” *IEEE Trans. Geosci. Remote Sens.*, vol. 63, pp. 1–15, 2025.

[15] H. Li, C. Xu, W. Yang, H. Yu, and G.-S. Xia, “Learning cross-

view visual geo-localization without ground truth,” *arXiv preprint arXiv:2403.12702*, 2024.

[16] L. Liu and H. Li, “Lending orientation to neural networks for cross-view geo-localization,” in *Proc. IEEE Conf. Comput. Vis. Pattern Recognit.*, 2019, p. 5624–5633.

[17] W. Hu, Y. Zhang, Y. Liang, Y. Yin, A. Georgescu, A. Tran, H. Kruppa, S.-K. Ng, and R. Zimmermann, “Beyond geo-localization: Fine-grained orientation of street-view images by cross-view matching with satellite imagery,” in *Proc. ACM Int. Conf. Multimedia*, 2022, p. 6155–6164.

[18] Y. Shi, X. Yu, L. Liu, T. Zhang, and H. Li, “Optimal feature transport for cross-view image geo-localization,” in *Proc. AAAI Conf. Artif. Intell.*, vol. 34, 2020, pp. 11 990–11 997.

[19] Y. Shi, L. Liu, X. Yu, and H. Li, “Spatial-aware feature aggregation for image based cross-view geo-localization,” in *Proc. Adv. Neural Inf. Process. Syst.*, vol. 32, p. 10090–10100, 2019.

[20] X. Zhang, X. Li, W. Sultani, Y. Zhou, and S. Wshah, “Cross-view geo-localization via learning disentangled geometric layout correspondence,” in *Proc. AAAI Conf. Artif. Intell.*, vol. 37, no. 3, 2023, pp. 3480–3488.

[21] W.-J. Ahn, S.-Y. Park, D.-S. Pae, H.-D. Choi, and M.-T. Lim, “Bridging viewpoints in cross-view geo-localization with siamese vision transformer,” *IEEE Trans. Geosci. Remote Sens.*, vol. 62, pp. 1–12, 2024.

[22] K. Regmi and M. Shah, “Bridging the domain gap for ground-to-aerial image matching,” in *Proc. IEEE Int. Conf. Comput. Vis.*, 2019, pp. 470–479.

[23] A. Toker, Q. Zhou, M. Maximov, and L. Leal-Taixe, “Coming down to earth: Satellite-to-street view synthesis for geo-localization,” in *Proc. IEEE Conf. Comput. Vis. Pattern Recognit.*, 2021, pp. 6488–6497.

[24] I. Goodfellow, J. Pouget-Abadie, M. Mirza, B. Xu, D. Warde-Farley, S. Ozair, A. Courville, and Y. Bengio, “Generative adversarial nets,” in *Proc. Adv. Neural Inf. Process. Syst.*, vol. 27, p. 2672–2680, 2014.

[25] X. Tian, J. Shao, D. Ouyang, and H. T. Shen, “UAV-satellite view synthesis for cross-view geo-localization,” *IEEE Trans. Circuits Syst. Video Technol.*, vol. 32, no. 7, pp. 4804–4815, 2021.

[26] F. Ge, Y. Zhang, Y. Liu, G. Wang, S. Coleman, D. Kerr, and L. Wang, “Multibranch joint representation learning based on information fusion strategy for cross-view geo-localization,” *IEEE Trans. Geosci. Remote Sens.*, vol. 62, pp. 1–16, 2024.

[27] H. Lv, H. Zhu, R. Zhu, F. Wu, C. Wang, M. Cai, and K. Zhang, “Direction-guided multi-scale feature fusion network for geo-localization,” *IEEE Trans. Geosci. Remote Sens.*, vol. 62, pp. 1–13, 2024.

[28] Y. Feng, J. Yu, F. Chen, Y. Ji, F. Wu, S. Liu, and X.-Y. Jing, “Visible-infrared person re-identification via cross-modality interaction transformer,” *IEEE Trans. Multimedia*, vol. 25, pp. 7647–7659, 2023.

[29] Y. Jiang, X. Cheng, H. Yu, X. Liu, H. Chen, and G. Zhao, “Dsaf: Dual space alignment framework for visible-infrared person re-identification,” *IEEE Trans. Multimedia*, vol. 27, pp. 5591–5603, 2025.

[30] M. Liu, Z. Zhang, Y. Bian, X. Wang, Y. Sun, B. Zhang, and Y. Wang, “Cross-modality semantic consistency learning for visible-infrared person re-identification,” *IEEE Trans. Multimedia*, vol. 27, pp. 568–580, 2025.

[31] X. Yu, N. Dong, L. Zhu, H. Peng, and D. Tao, “Clip-driven semantic

- discovery network for visible-infrared person re-identification,” *IEEE Trans. Multimedia*, vol. 27, pp. 4137–4150, 2025.
- [32] A. Radford, J. W. Kim, C. Hallacy, A. Ramesh, G. Goh, S. Agarwal, G. Sastry, A. Askell, P. Mishkin, J. Clark *et al.*, “Learning transferable visual models from natural language supervision,” in *Proc. Int. Conf. Mach. Learn.*, 2021, pp. 8748–8763.
- [33] Y. Bian, M. Liu, X. Wang, Y. Tang, and Y. Wang, “Occlusion-aware feature recover model for occluded person re-identification,” *IEEE Trans. Multimedia*, vol. 26, pp. 5284–5295, 2024.
- [34] H. Zhou, T. Luo, J. Zhang, and L. Liu, “Exploring the essence of relationships for scene graph generation via causal features enhancement network,” *IEEE Trans. Pattern Anal. Mach. Intell.*, vol. 47, no. 8, pp. 6616–6630, 2025.
- [35] Y. Liu and T. Luo, “Nonconvex and discriminative transfer subspace learning for unsupervised domain adaptation,” *Front. Comput. Sci.*, vol. 19, no. 2, p. 192307, 2025.
- [36] Y.-J. Li, X. Dai, C.-Y. Ma, Y.-C. Liu, K. Chen, B. Wu, Z. He, K. Kitani, and P. Vajda, “Cross-domain adaptive teacher for object detection,” in *Proc. IEEE Conf. Comput. Vis. Pattern Recognit.*, 2022, pp. 7581–7590.
- [37] N. Sun, T. Luo, W. Zhuge, H. Tao, C. Hou, and D. Hu, “Semi-supervised learning with label proportion,” *IEEE Trans. Knowl. Data Eng.*, vol. 35, no. 1, pp. 877–890, 2021.
- [38] B. Jiang, X. Wu, X. Zhou, Y. Liu, A. G. Cohn, W. Sheng, and H. Chen, “Semi-supervised multiview feature selection with adaptive graph learning,” *IEEE Trans. Neural Networks Learn. Syst.*, vol. 35, no. 3, pp. 3615–3629, 2022.
- [39] Z. Du, J. Li, H. Su, L. Zhu, and K. Lu, “Cross-domain gradient discrepancy minimization for unsupervised domain adaptation,” in *Proc. IEEE Conf. Comput. Vis. Pattern Recognit.*, 2021, pp. 3937–3946.
- [40] X. Wang, M. Liu, F. Wang, J. Dai, A.-A. Liu, and Y. Wang, “Relation-preserving feature embedding for unsupervised person re-identification,” *IEEE Trans. Multimedia*, vol. 26, pp. 714–723, 2024.
- [41] Y. Tao, J. Zhang, J. Hong, and Y. Zhu, “Dreamt: Diversity enlarged mutual teaching for unsupervised domain adaptive person re-identification,” *IEEE Trans. Multimedia*, vol. 25, pp. 4586–4597, 2023.
- [42] Z. Pang, L. Zhao, Q. Liu, and C. Wang, “Camera invariant feature learning for unsupervised person re-identification,” *IEEE Trans. Multimedia*, vol. 25, pp. 6171–6182, 2023.
- [43] H. Chen, B. Lagadec, and F. Bremond, “Ice: Inter-instance contrastive encoding for unsupervised person re-identification,” in *Proc. IEEE Int. Conf. Comput. Vis.*, 2021, pp. 14 960–14 969.
- [44] S. Xuan and S. Zhang, “Intra-inter camera similarity for unsupervised person re-identification,” in *Proc. IEEE Conf. Comput. Vis. Pattern Recognit.*, 2021, pp. 11 926–11 935.
- [45] Z. Dai, G. Wang, W. Yuan, S. Zhu, and P. Tan, “Cluster contrast for unsupervised person re-identification,” in *Proc. Asian Conf. Comput. Vis.*, 2022, pp. 1142–1160.
- [46] M. Ester, H.-P. Kriegel, J. Sander, X. Xu *et al.*, “A density-based algorithm for discovering clusters in large spatial databases with noise,” in *Proc. ACM SIGKDD Int. Conf. Knowl. Discov. Data Min.*, vol. 96, no. 34, 1996, pp. 226–231.
- [47] B. Yang, M. Ye, J. Chen, and Z. Wu, “Augmented dual-contrastive aggregation learning for unsupervised visible-infrared person re-identification,” in *Proc. ACM Int. Conf. Multimedia*, 2022, pp. 2843–2851.
- [48] B. Yang, J. Chen, and M. Ye, “Shallow-deep collaborative learning for unsupervised visible-infrared person re-identification,” in *Proc. IEEE Conf. Comput. Vis. Pattern Recognit.*, 2024, pp. 16 870–16 879.
- [49] Z. Liu, H. Mao, C.-Y. Wu, C. Feichtenhofer, T. Darrell, and S. Xie, “A convnet for the 2020s,” in *Proc. IEEE Conf. Comput. Vis. Pattern Recognit.*, 2022, pp. 11 976–11 986.
- [50] J. Hu, L. Shen, and G. Sun, “Squeeze-and-excitation networks,” in *Proc. IEEE Conf. Comput. Vis. Pattern Recognit.*, 2018, pp. 7132–7141.
- [51] A. v. d. Oord, Y. Li, and O. Vinyals, “Representation learning with contrastive predictive coding,” *arXiv preprint arXiv:1807.03748*, 2018.
- [52] B. Yang, M. Ye, J. Chen, and Z. Wu, “Augmented dual-contrastive aggregation learning for unsupervised visible-infrared person re-identification,” in *ACM MM*, 2022, p. 2843–2851.
- [53] A. Likas, N. Vlassis, and J. J. Verbeek, “The global k-means clustering algorithm,” *Pattern Recognit.*, vol. 36, no. 2, pp. 451–461, 2003.
- [54] H. Zhao, K. Ren, T. Yue, C. Zhang, and S. Yuan, “TransFG: A cross-view geo-localization of satellite and UAVs imagery pipeline using transformer-based feature aggregation and gradient guidance,” *IEEE Trans. Geosci. Remote Sens.*, vol. 62, pp. 1–12, 2024.
- [55] N. Keetha, A. Mishra, J. Karhade, K. M. Jatavallabhula, S. Scherer, M. Krishna, and S. Garg, “Anyloc: Towards universal visual place recognition,” *IEEE Rob. Autom. Lett.*, vol. 9, no. 2, pp. 1286–1293, 2023.
- [56] K. Garg, S. S. Puligilla, S. Kolathaya, M. Krishna, and S. Garg, “Revisit anything: Visual place recognition via image segment retrieval,” in *Proc. Eur. Conf. Comput. Vis.*, 2024, pp. 326–343.
- [57] M. Dai, E. Zheng, Z. Feng, L. Qi, J. Zhuang, and W. Yang, “Vision-based uav self-positioning in low-altitude urban environments,” *IEEE Trans. Image Process.*, vol. 33, pp. 493–508, 2024.
- [58] L. Van der Maaten and G. Hinton, “Visualizing data using t-SNE.” *J. Mach. Learn. Res.*, vol. 9, no. 11, pp. 2579–2605, 2008.